

Biospired Janus Silk E-Textiles with Wet–Thermal Comfort for Highly Efficient Biofluid Monitoring

Xuecheng He, Chuan Fan, Tailin Xu,* and Xueji Zhang*



Cite This: <https://doi.org/10.1021/acs.nanolett.1c03426>



Read Online

ACCESS |



Metrics & More



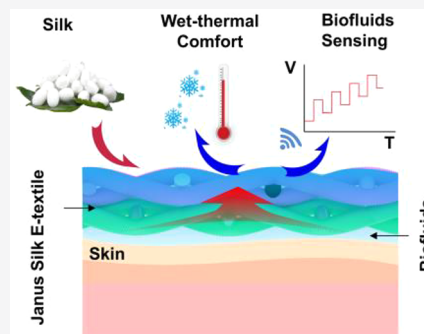
Article Recommendations



Supporting Information

ABSTRACT: Functionalized textiles capable of biofluid administration are favorable for enhancing the wet–thermal comfort of the wearer and healthcare performance. Herein, inspired by the Janus wettability of lotus leaf, we propose a skin-comfortable Janus electronic textile (e-textile) based on natural silk materials for managing and analysis of biofluid. Silk materials are chosen and modified as both a textile substrate and a sensing electrode due to its natural biocompatibility. The unidirectional biofluid behavior of such Janus silk substrate facilitates a comfortable skin microenvironment, including weakening the undesired wet adhesion ($\sim 0 \text{ mN cm}^{-2}$) and avoiding excessive heat or cold on the epidermis. We noninvasively analyze multiple targets of human sweat with less required liquid volume ($\sim 5 \mu\text{L}$) and a faster (2–3 min) response time based on the silk-based yarn electrode woven into the hydrophilic side of Janus silk. This work bridges the gap between physiological comfort and sensing technology using biomass-derived elements, presenting a new type of smart textiles for wet–thermal management and health monitoring.

KEYWORDS: bioinspired materials, silk, wet–thermal comfort, moisture management, sweat sensing



INTRODUCTION

The conformal noninvasive biointerface between sensors and the human epidermis is highly favorable for wearable electronics, leading to major advances in healthcare monitoring, personalized therapy, and human–machine interaction.^{1–5} However, existing wearable devices suffered from uncertain epidermal comfort or biocompatibility.^{6,7} Wet–thermal management is an important issue of wearable electronics and has profound impact upon skin comfort,^{8,9} which can be enhanced by tailoring their interfacial wicking behavior, especially those e-textiles used in damp settings such as humidity,¹⁰ urine,¹¹ and sweat electronics.^{12,13} In most traditional fabrics, the wicking behavior is bidirectional; in other words, moisture can be delivered from the epidermis to the environment as well as the opposite direction. Construction of an anisotropic surface geometry,^{9,14} with roughness¹⁵ and wettability,^{16,17} is an effective strategy to achieve unidirectional biofluid administration.¹⁸ These functionalized textiles have shown great potential in reducing an undesired wet and sticky experience, accelerating water evaporation, and tailoring body temperature,^{9,19} which is extremely valuable in creating a comfortable skin microenvironment for smart clothing.

Silkworm silk, an ancient natural fiber known as skin-friendly clothing for centuries, is playing an important role in emerging research area of e-textiles.^{20,21} In contrast to artificial polymer fibers, silk materials have the distinct advantages of biocompatibility, biodegradability, light weight, mechanical

robustness, and so on. Several advanced functionalized materials, silk fiber/yarns,^{22,23} textile,²⁴ and films,^{25,26} have been developed as biosupports of e-textiles via physical and chemical techniques for long-term wearability and clinical applications. In addition, silk fibroin as the main component (70–80 wt %) of silkworm cocoon, can also participate in the formation of an active component of flexible and biocompatible electronics in an intrinsic^{27–29} or carbonized manner.^{30,31} The varied morphologies and modification strategies for silk materials are expected to furnish options for designing a wet–thermal comfort e-textile. However, simultaneous functionality of skin comfort and healthcare based on silk biomaterials is still rare, since it is challenging to combine these merits by a single material-modification technique.

In this paper, we developed a bioinspired silk-based Janus electronic sportswear with personal wet–thermal comfort as well as highly effective biofluid analysis. Intrinsically hydrophilic (with water contact angle, viz., WCA of 0° , Figure S1) silk fabric successively is subjected to a chemical bath of a hydrophobic solution and single-side plasma treatment, creating hydrophobicity (WCA of $139 \pm 2.1^\circ$)-hydrophilicity

Received: September 4, 2021

Revised: October 12, 2021

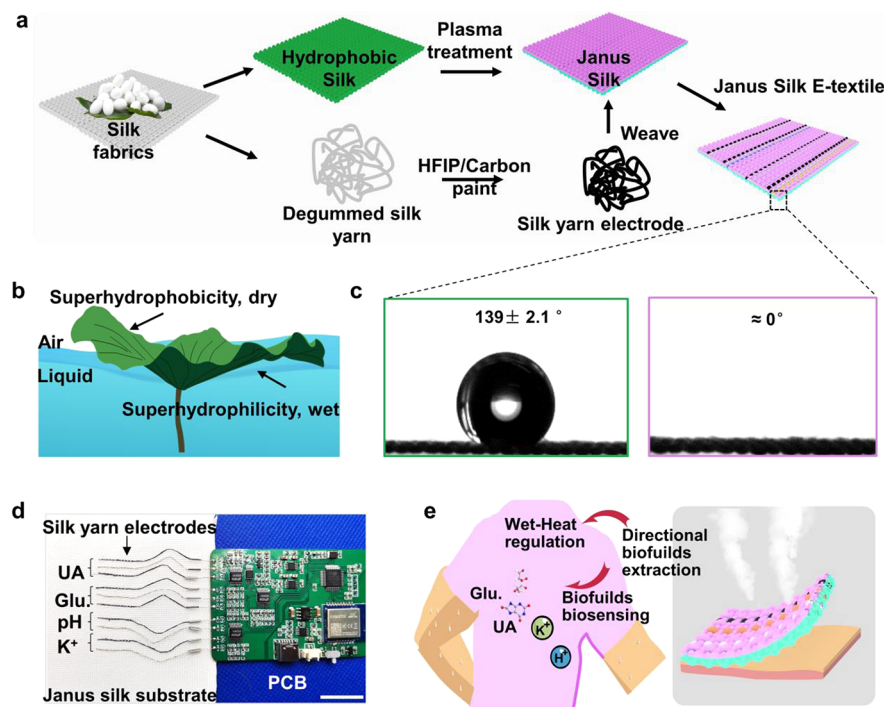


Figure 1. Design of Janus silk e-textile for unidirectional biofluid management and monitoring. (a) Schematic of fabrication process of Janus silk e-textile, including fabrication of Janus silk biosupport, silk yarn electrode, and weaving of silk yarn electrode onto the hydrophilic side of Janus silk substrate. (b) Schematic illustrating the Janus wettability of a natural lotus leaf, where upper and lower surfaces are superhydrophobic and superhydrophilic, respectively. (c) WCA of hydrophobic and hydrophilic surface of the Janus silk. (d) Optical image of a PCB-connected Janus silk e-textile. Scale bar: 1 cm. (e) Schematic of the Janus silk e-textile functionalized with comfort wearing experience (biofluid extraction, wet–heat regulation) and multiplexed biosensing.

(WCA of 0°) gradient on the opposite layer of the silk substrate (Figures 1a,c). Such Janus wettability mimics the asymmetric structure of the lotus leaf, which remains dry on the hydrophobic side and wet on the hydrophilic side (Figure 1b). However, silk-based electrodes are achieved by incorporating conductive carbon paint onto hexafluoroisopropanol (HFIP)-stabilized-degummed silk yarn. The resulting conductive silk yarn is selectively woven into the hydrophilic side of the above Janus silk substrate as biofluid-sensing electrodes and connected to a printed circuit board (PCB, Figure 1d) for data recording, processing, and transmission. The synergistic effect of the Janus silk substrate and silk yarn electrodes can not only unidirectionally remove excessive biofluid from the skin and thereby create a comfortable epidermis microclimate (eliminating a wet and sticky environment, regulating body temperature, etc.) but also contribute to multiplexed biofluid analysis with a lower volume and faster response compared to conventional fabric materials (Figure 1e). Through this work, we aim to unveil the delicate relationship among unidirectional biofluid wicking, a comfortable physiological microenvironment, and sensing performance.

RESULT AND DISCUSSION

Unidirectional Water Transport Properties and Mechanism of the Janus Silk Substrate. Commercial silk textile is essentially made of fibroin, which has abundant functional groups, such as hydroxyl groups in the amino acid residues (e.g., serine) linked with peptide bonds.³² Hydroxyl groups have proved capable of providing reaction sites with a silane coupling agent.³³ Here, we adopted a simple hydro-

phobization strategy for silk textile by dip-coating it in an octadecyltrichlorosilane (OTS) solution, where the microscopic mechanism is shown in Figure 2a. Briefly, the modification process is based on a typical hydrolysis reaction involving formation of a Si–O bond between hydroxyl of fibroin and OTS. Raw silk textile was made of smooth fiber with diameter ranges from 150 to 300 μm (Figure 2b). After modification, the hydrophobic silk showed a much rougher surface (Figure 2c), and its element components were confirmed in X-ray photoelectron spectroscopy (XPS) in Figure 2d. Beyond abundant C, N, and O elements, weak peaks of Si ($\sim 103, 154$ eV) and Cl (~ 198 eV) emerged in the spectra of the modified silk material. Figure 2e shows the Gaussian-fitted high-resolution Si 2p spectrum, wherein the low binding energy around 102.7 eV is from the intrinsic Si–C bond of OTS.³⁴ Another peak can be found about 103.8 eV corresponding to the Si–O bond, which can be attributed to the successful coupling link between fibroin and OTS.³⁵

Janus silk with opposite wettability was constructed by one-side plasma treatment for directional moisture wicking. Once touched by the hydrophobic surface, water rapidly passed through and wetted the other hydrophilic side. By comparison, the microdroplet spread as soon as it contacted the hydrophilic silk side without penetrating the hydrophilic silk surface (Figure 2f and Movie S1). Such wettability differences were also confirmed by immersing the Janus silk into blue ink. The hydrophilic layer showed a much higher wicking height (Figures S2a) and larger spreading diameters (Figures S2b,c) than the hydrophobic surface, regardless of the droplet volume from 20 to 200 μL . We attempt to understand the mechanism of asymmetric wicking property of such a Janus silk biosupport

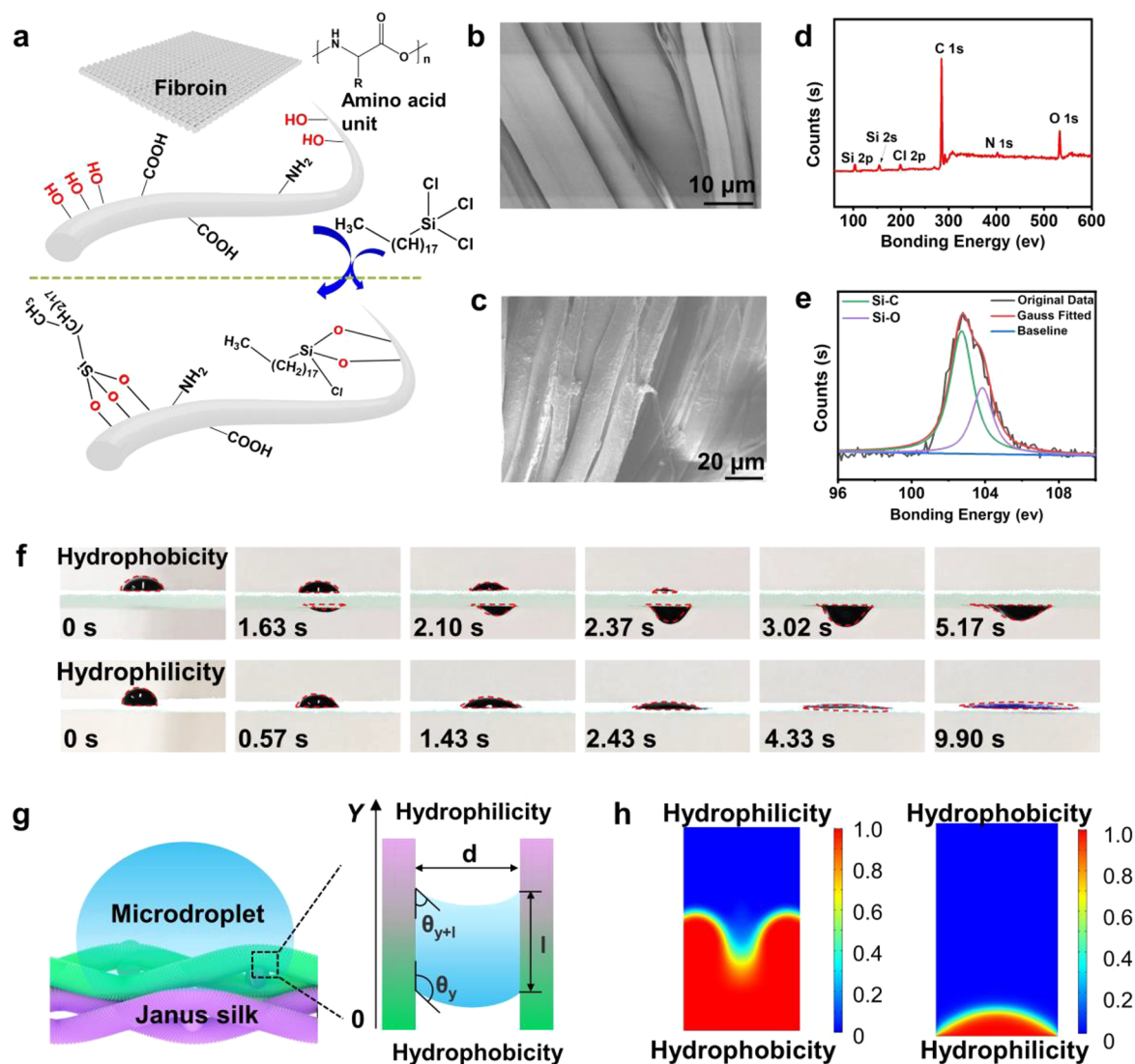


Figure 2. Unidirectional moisture-wicking phenomenon and mechanism of Janus silk biosupport. (a) Schematic of the chemical reaction between OTS and silk fibroin. SEM images of silk textile (b) before and (c) after OTS modification. (d) XPS of OTS-functionalized silk textile and (e) corresponding high-resolution Si 2p spectrum. (f) Time-lapse images showing the phenomenon of unidirectional water transportation (all the images originated from [Movie S1](#)). (g) Capillary model for understanding the driving force toward water droplet inside the Janus silk and (h) the corresponding finite element simulations.

by a theoretical explanation and finite element analysis (FAS). To simplify these analyses, we hypothesize that the microcosmic interface between moisture and silk fabrics is a capillary model with gradient wettability. Both of the two analytical outcomes ([Figures 2g,h](#) and [S3](#) and [Movie S2](#)) show that liquid can fill the capillary from hydrophobic to hydrophilic side, and not vice versa (the analytical process were detailed in the [Experimental Section of Supporting Information](#)).

Unidirectional Biofluid Wicking for Comfortable Wearable Somatosensor. The wearing of a somatosensor of the Janus silk biosupport was experimentally examined, involving local epidermis humidity, skin adhesion in wet conditions, and thermal management. Prior to applying it to a human epidermis, we assessed the cytotoxicity of the silk materials. [Figure 3a](#) illustrates fluorescence microscopy images of stained NHDF cells in blank and Janus silk groups after 24 h of incubation. The two groups of cells showed comparable morphology and quantity, and a similar phenomenon was also observed in MCF-7 cells ([Figure S4](#)). We then compared the

on-body sweat absorption performance of pristine silk and Janus silk. Both fabrics were attached on a volunteer's sweaty forearm for 1 min and then uncovered. A certain amount of sweat remained on the epidermis, especially at the boundary between bare silk and skin ([Figure 3b](#), top). However, the skin faced with the hydrophobic side of Janus silk was almost dry, and no obvious perspiration remained ([Figure 3b](#), bottom). The local relative humidity of the Janus silk (~67, 52, and 62%) significantly decreased in all three individuals compared to that of pristine silk (~78, 66, and 75%, [Figure 3c](#)). Conventional wetted textiles involving pristine silk, cotton, polyester, and wool showed varying degrees of skin adhesion force ranging from 14.6 to 18.5 mN cm⁻². By comparison, the Janus silk clothing possessed a negligible epidermis adhesion force (low to around 0 mN cm⁻²; [Figure 3d](#)). These data indicated that a dry interface between Janus silk biosupport and the human epidermis was formed, where unfavorable wet sticking was eliminated.

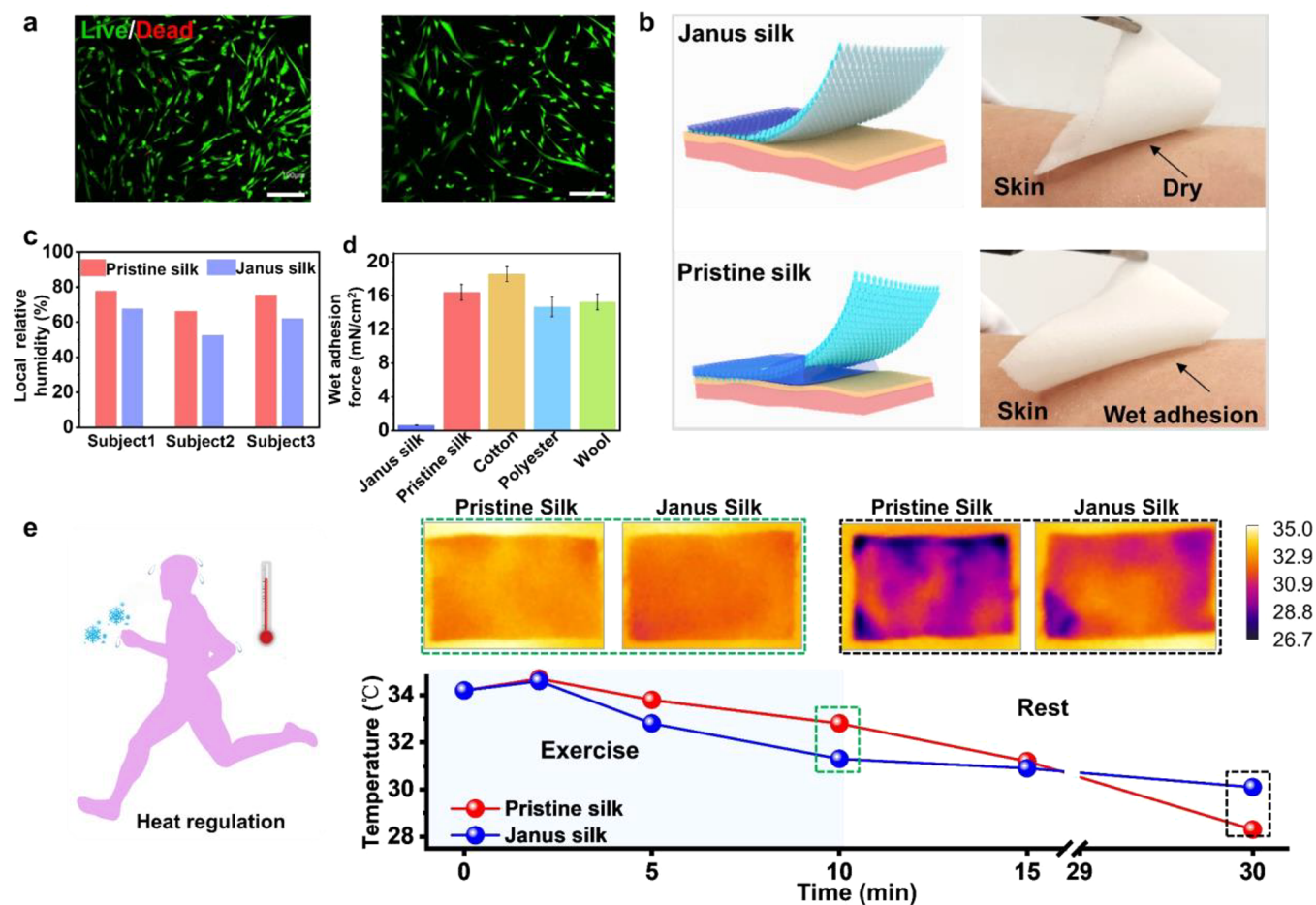


Figure 3. Characterization of wearing of the somatosensor of Janus silk clothing. (a) Typical fluorescence microscopy image showing the live/dead assay of NHDF cells after incubation for 24 h with different silk materials. Scale bar: 200 μm . (b) On-body sweat absorbance between pristine and Janus silk. (c) Local relatively humidity of the skin after covering with pristine and Janus silk. (d) Wet adhesion force of Janus silk and various conventional fabrics. (e) Temperature of the pristine and Janus silk on wetted epidermis over exercise and rest periods.

Thermal management by fabrics is another significant factor of epidermal comfort. Figure 3e plots a whole temperature evolution trend of the silk clothing placed on human skin as a function of time, including exercise and rest stages. In the exercise stage (from 0 to 10 min), the temperature of area covered by Janus silk surface was slightly lower than that of the pristine silk surface (e.g., ~ 1.5 $^{\circ}\text{C}$ lower at 10 min). The potential reason could be that sweat generated during the exercise period was delivered and diffused to the outer hydrophilic layer of Janus silk, therefore accelerating the evaporation rate and taking away excessive heat.¹⁹ In the rest stage (from 10 to 30 min), conversely, the average temperature of the area covered by Janus silk was generally higher (e.g., ~ 1.8 $^{\circ}\text{C}$ higher at 30 min) than that of pristine silk. In the rest stage, biofluid completely evaporated from the Janus silk but remained inside the pristine silk. As a result, the dry Janus silk has a lower thermal conductivity compared to that of wet pristine silk,³⁶ providing a warmer wearing experience than the traditional fabrics when rest.

Characterization of the Integrated Janus Silk E-Textile. Following biofluid wicking analysis, the electronic elements of the Janus silk e-textile were then systematically investigated. Figure 4a displays the schematic fabrication of the conductive silk yarn electrodes. Commercial degummed silk yarns were first incubated with HFIP in airtight containers at 60 $^{\circ}\text{C}$ for 24 h followed by coating commercial carbon paint

(carbon black as main conductive ingredient, see the Experimental Section in Supporting Information). HFIP was used to partially dissolve the surface of the degummed silk yarns according to previous works.^{37,38} Therefore, the adhesion force between silk yarns and carbon ink were further enhanced, and the electrical resistance maintained stable after bending up to 800 cycles (Figure S5). Although the commercial carbon paint used in this work was highly viscous (Figure S6a), the silk yarn with a direct coating of carbon paint (without HFIP treatment) was vulnerable to external mechanical deformation, whose electrical resistance significantly increased upon applying only 200 bending cycles. On the basis of the above dip-coating process, the as-prepared silk yarn electrode can be continuously wound onto a roller (Figure S6b) after drying. Figure S7 demonstrates the SEM images of resulting electrode inat different magnifications, where the silk yarn coated with a dense carbon layer could be clearly observed. Two strands of yarns were combined for generating higher electrochemical capacity as revealed in the cyclic voltammetry (CV) measurement in Figure S8. The whole system demonstrated fine structural integrity without any detachment of the woven silk yarn under stretching, folding, and rolling (Figure S9). SEM images in Figure 4b show that the carbon-paint-coated silk fiber was merely woven into the top layer (hydrophilic side) of the silk biosupport and tightly bound with whole textile substrate. The pristine textile and Janus silk e-textile showed

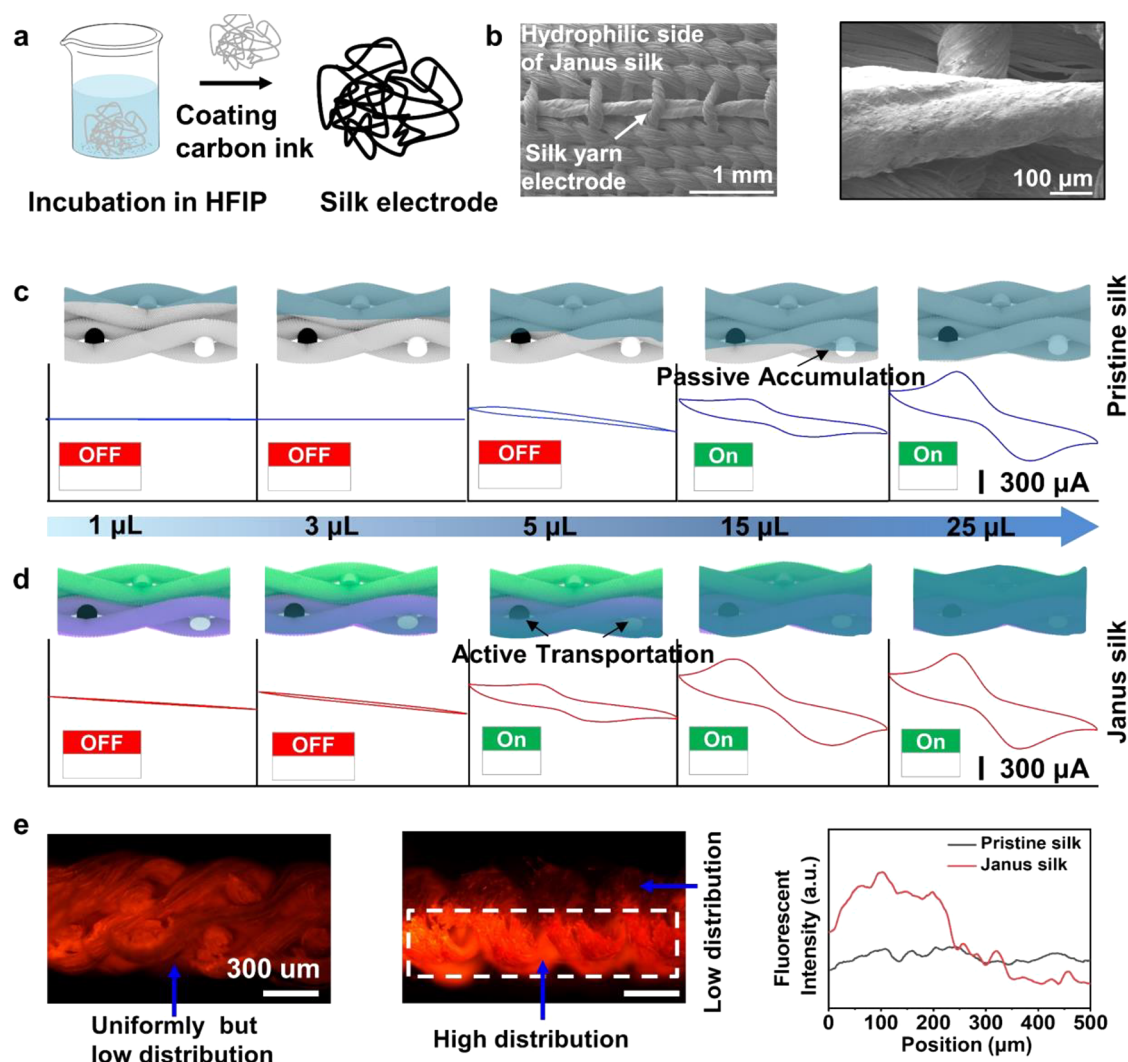


Figure 4. Characterizations of the silk yarn electrodes. (a) Schematic of conductive silk yarn electrode fabrication, including incubation in HFIP and coated with carbon ink. (b) SEM image of the corresponding enlarged view of silk yarn electrode just woven onto the hydrophilic side of silk fabric. CVs in different amount (1, 3, 5, 15, and 25 μL) of electrolyte solutions (containing 5 mM $[\text{Fe}(\text{CN})_6]^{3-}$ and 0.4 M KCl, scan rate of 200 mV s^{-1} with a commercial Ag/AgCl electrode) onto (c) pristine and (d) Janus silk. (e) Cross-sectional fluorescence image and intensity analysis showing vertical distribution of moisture in pristine and Janus silk, respectively.

similar mechanical curves upon tensile strength test. The corresponding endurable tensile force and elongation at break were 187.64 and 186.76 N and 67.95 and 61.93%, respectively (Figure S10), indicating that all the modification procedures did not affect the internal structure and mechanical properties of the silk fibers.

One distinct advantage of such Janus e-textile system lies on their low-volume biosensing, which was investigated by a volume-dependent cyclic voltammetry CV experiment. As illustrated in Figure 4c,d, $[\text{Fe}(\text{CN})_6]^{3-}$ redox peaks generally increased along with the applied solution volume. However, the required solution volume was different in pristine and Janus silk. A 5 μL aliquot of $[\text{Fe}(\text{CN})_6]^{3-}$ solution was just enough for the electrode woven in the hydrophilic side of Janus silk to generate obvious redox peaks. By comparison, in the case of the electrodes woven in pristine silk, 15 μL was the lowest amount necessary to observe similar CV curves (Figure 4c). Therefore, the critical volume threshold for available electrochemical signal was remarkably reduced from 15 to 5 μL (Figure 4d) after modification with Janus wettability. To

further verify this outcome, 5 μL of rhodamine B solution was added as a tracer dye to visualize the moisture distribution in the cross section of two silk materials (Figure 4e). Apparently, in pristine silk, the dyestuff exhibited a homogeneous but relatively low distribution, while higher moisture accumulation on the hydrophilic side of Janus silk was observed. The fluorescent intensity of 0–250 μm was remarkably higher than that of 250–500 μm .

The electrochemical performances of each silk-based yarn sensor were individually examined with respective analyte solutions based on initial or modified silk yarn electrode systems (Figure S11). The modified active layers on silk fiber were shown in the SEM images in Figure S12. UA (0–200 μM) could be directly analyzed with differential pulse voltammetry (DPV, current peaks at ~ 0.39 V),³⁹ and glucose was measured chronoamperometrically in 0–250 μM glucose solutions (Figure 5a,b). The corresponding calibration curves exhibited favorable linearity and sensitivity (1.703 and 0.49 $\text{nA}/\mu\text{M}$ for UA and glucose, respectively). Potentiometric responses of the pH and K^+ sensors were recorded in

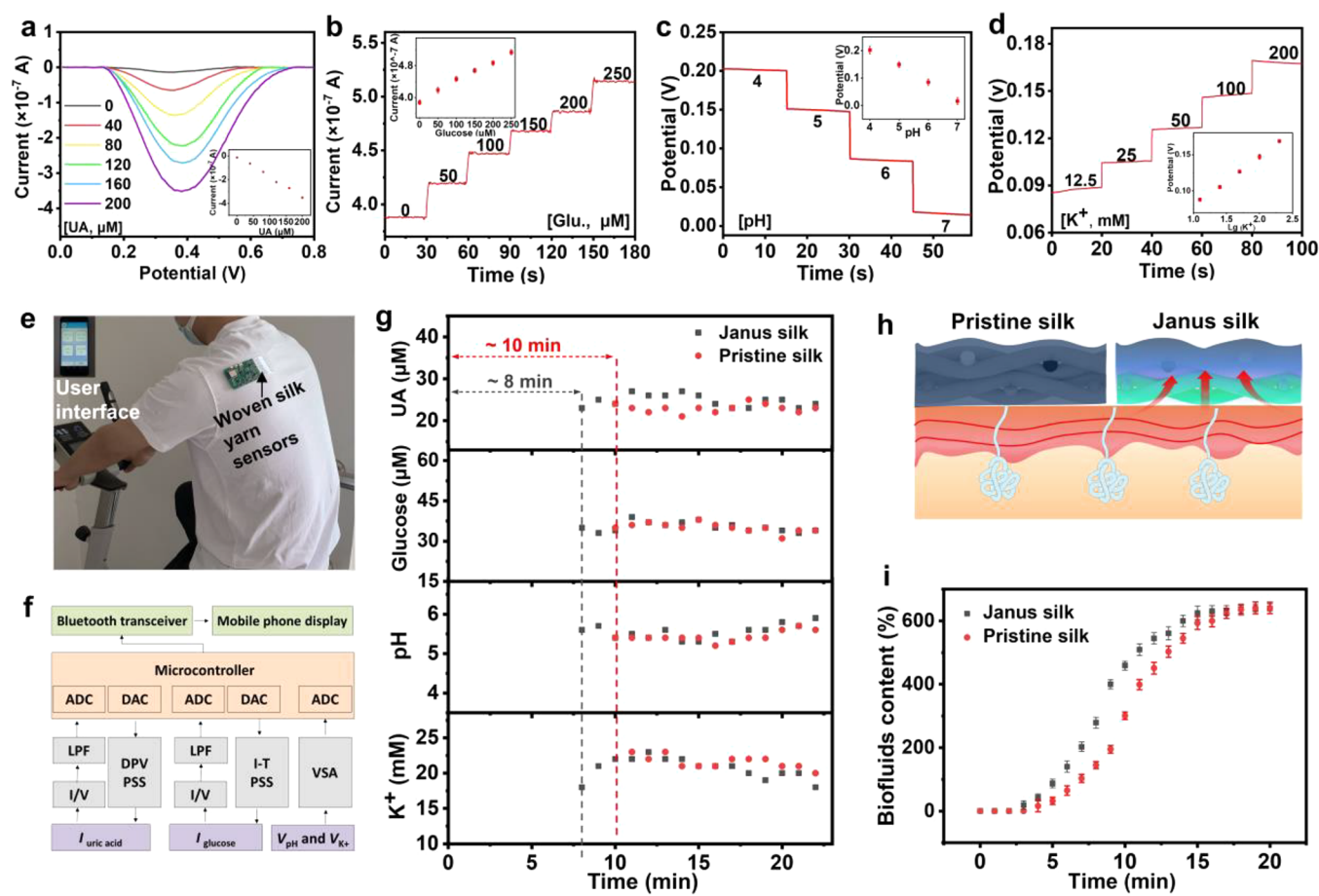


Figure 5. On-body evaluation of the Janus silk e-textile toward personalized sweat management and monitoring. Electrochemical sensing curves of each sensor, including DPV and chronoamperometric responses of (a) UA and (b) glucose, as well as OCP responses of (c) pH and (d) K^+ , respectively. Insets: the corresponding calibration plots of each sensor. (e) Photograph of a volunteer wearing Janus silk e-textile, where silk yarn electrode was linked with a PCB on the shoulder during cycling exercise. (f) System-level block diagram of the PCB. (g) Discrete and multiplexed detection of UA, glucose, pH, and K^+ in the sweat with Janus silk and neighboring pristine silk. (h) Schematic showing that for collecting given sweat volume on electrode the required time on Janus silk is less than that on pristine silk due to the unidirectional moisture wicking behavior. (i) Schematic and actual measurement of sweat content on the electrode side of Janus silk and neighboring pristine silk region by MMT.

respective standard solutions (open circuit potential, OCP) with pH of 4–7 and K^+ of 12.5–200 mM, respectively (Figure 5c,d). Quasi-near-Nernstian sensitivities of 62.25 mV/lg (H^+) and 67.44 mV/lg (K^+) were also observed.⁴⁰ These sensors also showed fine selectivity and reproducibility, as shown in Figures S13 and S14.

On-Body Evaluation of the Integrated Janus Silk E-Textile. On-body biofluid sensing was finally carried out to assess the feasibility and versatility of the Janus e-textile as a comfortable smart sportswear. A healthy volunteer who wore the silk clothing was asked to exercise on a stationary bicycle in an ambient setting (Figure 5e). Only local silk fabrics were modified with Janus wettability, and other domains remained as pristine silk to better compare their sensing performances. Discrete variations in sweat UA, glucose, pH, and K^+ were recorded by a connected PCB once a minute, where the PCB can be closed attached to the textile without any detachment using a double-sided adhesive tape. The collected data further underwent signal transduction, conditioning, processing, and wireless transmission onto a smartphone (Figure 5f). In general, similar concentration ranges of these sweat markers throughout the exercise were observed in the electrode woven in the Janus silk and the neighboring pristine silk region. However, the response times were different. For Janus silk,

readouts were available after about 8 min of exercise, a shorter time than that of the neighboring pristine silk zone (~10 min, Figure 5g). To explain this bioassay difference, the biofluid contents on the electrode side during the exercise period were recorded by a moisture-management tester (MMT, Figure 5h,i). The biofluid content continuously increased until the hydrophilic side was saturated. During this process, the sweat content on the electrode side of the Janus silk was generally higher than that of pristine silk. Thus, for a given amount of sweat on the electrode side, the required collection or response time at the same exercise intensity and body parts was reduced in Janus silk. These results prove that our Janus silk e-textile could perform on-body monitoring task and more importantly, accelerate sweat sampling and analytical efficiency by benefiting from its unidirectional water-wicking property compared to that of traditional clothing.

CONCLUSION

In conclusion, this study proposed a silk-based sportswear that optimizes skin comfort and electrochemical-sensing performance. The anisotropic wettable material was constructed on a silk fabric substrate, providing directional biofluid wicking accompanied by pleasant wet–thermal comfort. HFIP-

stabilized and carbon-modified silk yarn electrodes were woven in the hydrophilic side and served as the electrochemical sensing element. The unidirectional biofluid transport from the hydrophobic side to the hydrophilic side of the silk yarn electrode created a comfortable physiological microenvironment by tailoring epidermal humidity and temperature and allowed for biofluid sensing. As an example of downstream application, multiple sweat targets such as UA, glucose, pH, and K^+ were analyzed and wirelessly transmitted onto a user interface by integrated circuit techniques with reduced biofluid volume and wicking time. Given the versatile design mechanism, it is expected that such a comfortable Janus silk e-textile can be reconfigured into new type of wound dressing, disposable diaper, and breathing mask for probing the health status and clinical requirement of individuals and society.

■ ASSOCIATED CONTENT

SI Supporting Information

The Supporting Information is available free of charge at <https://pubs.acs.org/doi/10.1021/acs.nanolett.1c03426>.

Detailed information about the fabrication and characterization of Janus silk e-textile, theoretical simulation and FAS of unidirectional moisture wicking, sensing strategies (PDF)

Movies S1 and S2: Actual and stimulated models of unidirectional moisture-wicking phenomenon of the device (MP4, MP4)

■ AUTHOR INFORMATION

Corresponding Authors

Tailin Xu – School of Biomedical Engineering, Health Science Center, Shenzhen University, Shenzhen 518060, PR China; orcid.org/0000-0003-4037-2856; Email: xutailin@szu.edu.cn

Xueji Zhang – School of Biomedical Engineering, Health Science Center, Shenzhen University, Shenzhen 518060, PR China; Email: zhangxueji@szu.edu.cn

Authors

Xuecheng He – School of Biomedical Engineering, Health Science Center, Shenzhen University, Shenzhen 518060, PR China; Beijing Advanced Innovation Center for Materials Genome Engineering, Research Center for Bioengineering and Sensing Technology, University of Science and Technology Beijing, Beijing 100083, PR China; orcid.org/0000-0003-3702-8915

Chuan Fan – School of Biomedical Engineering, Health Science Center, Shenzhen University, Shenzhen 518060, PR China; Beijing Advanced Innovation Center for Materials Genome Engineering, Research Center for Bioengineering and Sensing Technology, University of Science and Technology Beijing, Beijing 100083, PR China

Complete contact information is available at: <https://pubs.acs.org/doi/10.1021/acs.nanolett.1c03426>

Author Contributions

H.X., F.C., X.T., and Z.X. conceived and designed the experiments. H.X. and F.C. prepared materials, carried out the experiments, and analyzed the experimental data. H.X. wrote the manuscript. X.T. and Z.X. supervised all the aspects of this work and provided financial support. All authors discussed the results and contributed to the paper.

Notes

The authors declare no competing financial interest.

■ ACKNOWLEDGMENTS

The authors acknowledge funding from National Natural Science Foundation of China (21804007 and 21890742), SZU Top Ranking Project (86000000210), and Shenzhen Stability Support Plan (20200806163622001).

■ REFERENCES

- (1) Ray, T. R.; Choi, J.; Bandodkar, A. J.; Krishnan, S.; Gutruf, P.; Tian, L. M.; Ghaffari, R.; Rogers, J. A. Bio-Integrated Wearable Systems: A Comprehensive Review. *Chem. Rev.* **2019**, *119*, 5461–5533.
- (2) Yang, Y.; Gao, W. Wearable and flexible electronics for continuous molecular monitoring. *Chem. Soc. Rev.* **2019**, *48*, 1465–1491.
- (3) Gao, W.; Emaminejad, S.; Nyein, H. Y. Y.; Challa, S.; Chen, K.; Peck, A.; Fahad, H. M.; Ota, H.; Shiraki, H.; Kiriya, D.; Lien, D. H.; Brooks, G. A.; Davis, R. W.; Javey, A. Fully integrated wearable sensor arrays for multiplexed in situ perspiration analysis. *Nature* **2016**, *529*, 509–514.
- (4) Kim, D. H.; Lu, N.; Ma, R.; Kim, Y. S.; Kim, R. H.; Wang, S.; Wu, J.; Won, S. M.; Tao, H.; Islam, A.; Yu, K. J.; Kim, T. I.; Chowdhury, R.; Ying, M.; Xu, L.; Li, M.; Chung, H. J.; Keum, H.; McCormick, M.; Liu, P.; Zhang, Y. W.; Omenetto, F. G.; Huang, Y.; Coleman, T.; Rogers, J. A. Epidermal electronics. *Science* **2011**, *333*, 838–843.
- (5) Miyamoto, A.; Lee, S.; Cooray, N. F.; Lee, S.; Mori, M.; Matsuhisa, N.; Jin, H.; Yoda, L.; Yokota, T.; Itoh, A.; Sekino, M.; Kawasaki, H.; Ebihara, T.; Amagai, M.; Someya, T. Inflammation-free, gas-permeable, lightweight, stretchable on-skin electronics with nanomeshes. *Nat. Nanotechnol.* **2017**, *12*, 907–913.
- (6) Babar, A. A.; Miao, D.; Ali, N.; Zhao, J.; Wang, X.; Yu, J.; Ding, B. Breathable and Colorful Cellulose Acetate-Based Nanofibrous Membranes for Directional Moisture Transport. *ACS Appl. Mater. Interfaces* **2018**, *10*, 22866–22875.
- (7) Chao, M.; He, L.; Gong, M.; Li, N.; Li, X.; Peng, L.; Shi, F.; Zhang, L.; Wan, P. Breathable Ti3C2Tx MXene/Protein Nanocomposites for Ultrasensitive Medical Pressure Sensor with Degradability in Solvents. *ACS Nano* **2021**, *15*, 9746–9758.
- (8) Li, Q.; Chen, G.; Cui, Y.; Ji, S.; Liu, Z.; Wan, C.; Liu, Y.; Lu, Y.; Wang, C.; Zhang, N.; Cheng, Y.; Zhang, K. Q.; Chen, X. Highly Thermal-Wet Comfortable and Conformal Silk-Based Electrodes for On-Skin Sensors with Sweat Tolerance. *ACS Nano* **2021**, *15*, 9955–9966.
- (9) Dai, B.; Li, K.; Shi, L.; Wan, X.; Liu, X.; Zhang, F.; Jiang, L.; Wang, S. Bioinspired Janus Textile with Conical Micropores for Human Body Moisture and Thermal Management. *Adv. Mater.* **2019**, *31*, 1904113.
- (10) Ma, L.; Wu, R.; Patil, A.; Zhu, S.; Meng, Z.; Meng, H.; Hou, C.; Zhang, Y.; Liu, Q.; Yu, R.; Wang, J.; Lin, N.; Liu, X. Y. Full-Textile Wireless Flexible Humidity Sensor for Human Physiological Monitoring. *Adv. Funct. Mater.* **2019**, *29*, 1904549.
- (11) He, X.; Pei, Q.; Xu, T.; Zhang, X. Smartphone-based tape sensors for multiplexed rapid urinalysis. *Sens. Actuators, B* **2020**, *304*, 127415.
- (12) Wang, L.; Wang, L.; Zhang, Y.; Pan, J.; Li, S.; Sun, X.; Zhang, B.; Peng, H. Weaving Sensing Fibers into Electrochemical Fabric for Real-Time Health Monitoring. *Adv. Funct. Mater.* **2018**, *28*, 1804456.
- (13) He, X.; Yang, S.; Pei, Q.; Song, Y.; Liu, C.; Xu, T.; Zhang, X. Integrated Smart Janus Textile Bands for Self-Pumping Sweat Sampling and Analysis. *ACS Sens.* **2020**, *5*, 1548–1554.
- (14) Wang, X.; Huang, Z.; Miao, D.; Zhao, J.; Yu, J.; Ding, B. Biomimetic Fibrous Murray Membranes with Ultrafast Water Transport and Evaporation for Smart Moisture-Wicking Fabrics. *ACS Nano* **2018**, *13*, 1060–1070.

- (15) Xu, J.; Du, X.; Xin, B.; Kan, C.; Xiao, Y.; Chen, Z.; Zhou, M.; Yan, Q. Moisture-Wicking and Solar-Heated Coaxial Fibers with a Bark-like Appearance for Fabric Comfort Management. *ACS Appl. Mater. Interfaces* **2021**, *13*, 26590.
- (16) Wang, Y.; Liang, X.; Zhu, H.; Xin, J. H.; Zhang, Q.; Zhu, S. Reversible Water Transportation Diode: Temperature-Adaptive Smart Janus Textile for Moisture/Thermal Management. *Adv. Funct. Mater.* **2020**, *30*, 1907851.
- (17) Miao, D.; Huang, Z.; Wang, X.; Yu, J.; Ding, B. Continuous, Spontaneous, and Directional Water Transport in the Trilayered Fibrous Membranes for Functional Moisture Wicking Textiles. *Small* **2018**, *14*, 1801527.
- (18) Liu, M.; Wang, S.; Jiang, L. Nature-inspired superwettability systems. *Nat. Rev. Mater.* **2017**, *2*, 17036.
- (19) Yang, S.; Zhu, Z.; Wu, Z.; Wu, J.; Yin, K. Femtosecond laser rapid fabrication of Janus sweat-permeable fabric for personal cooling. *Appl. Phys. Lett.* **2020**, *117*, 213701.
- (20) Wang, C.; Xia, K.; Zhang, Y.; Kaplan, D. L. Silk-Based Advanced Materials for Soft Electronics. *Acc. Chem. Res.* **2019**, *52*, 2916–2927.
- (21) Shao, Z.; Vollrath, F. Surprising strength of silkworm silk. *Nature* **2002**, *418*, 741–741.
- (22) Muller, C.; Hamed, M.; Karlsson, R.; Jansson, R.; Marcilla, R.; Hedhammar, M.; Inganas, O. Woven electrochemical transistors on silk fibers. *Adv. Mater.* **2011**, *23*, 898–901.
- (23) Ye, C.; Ren, J.; Wang, Y.; Zhang, W.; Qian, C.; Han, J.; Zhang, C.; Jin, K.; Buehler, M. J.; Kaplan, D. L.; Ling, S. Design and Fabrication of Silk Templated Electronic Yarns and Applications in Multifunctional Textiles. *Matter* **2019**, *1*, 1411–1425.
- (24) Liu, Y.; Tao, L. Q.; Wang, D. Y.; Zhang, T. Y.; Yang, Y.; Ren, T. L. Flexible, highly sensitive pressure sensor with a wide range based on graphene-silk network structure. *Appl. Phys. Lett.* **2017**, *110*, 123508.
- (25) Ling, S.; Jin, K.; Kaplan, D. L.; Buehler, M. J. Ultrathin Free-Standing Bombyx mori Silk Nanofibril Membranes. *Nano Lett.* **2016**, *16*, 3795–800.
- (26) Kim, D. H.; Viventi, J.; Amsden, J. J.; Xiao, J.; Vigeland, L.; Kim, Y. S.; Blanco, J. A.; Panilaitis, B.; Frechette, E. S.; Contreras, D.; Kaplan, D. L.; Omenetto, F. G.; Huang, Y.; Hwang, K. C.; Zakin, M. R.; Litt, B.; Rogers, J. A. Dissolvable films of silk fibroin for ultrathin conformal bio-integrated electronics. *Nat. Mater.* **2010**, *9*, 511–517.
- (27) Liang, X.; Li, H.; Dou, J.; Wang, Q.; He, W.; Wang, C.; Li, D.; Lin, J. M.; Zhang, Y. Stable and Biocompatible Carbon Nanotube Ink Mediated by Silk Protein for Printed Electronics. *Adv. Mater.* **2020**, *32*, 2000165.
- (28) Zhang, M.; Zhao, M.; Jian, M.; Wang, C.; Yu, A.; Yin, Z.; Liang, X.; Wang, H.; Xia, K.; Liang, X.; Zhai, J.; Zhang, Y. Printable Smart Pattern for Multifunctional Energy-Management E-Textile. *Matter* **2019**, *1*, 168–179.
- (29) Ling, S.; Wang, Q.; Zhang, D.; Zhang, Y.; Mu, X.; Kaplan, D. L.; Buehler, M. J. Integration of stiff graphene and tough silk for the design and fabrication of versatile electronic materials. *Adv. Funct. Mater.* **2018**, *28*, 1705291.
- (30) Wang, C.; Li, X.; Gao, E.; Jian, M.; Xia, K.; Wang, Q.; Xu, Z.; Ren, T.; Zhang, Y. Carbonized Silk Fabric for Ultrastretchable, Highly Sensitive, and Wearable Strain Sensors. *Adv. Mater.* **2016**, *28*, 6640–6648.
- (31) Wang, C.; Xia, K.; Zhang, M.; Jian, M.; Zhang, Y. An All-Silk-Derived Dual-Mode E-skin for Simultaneous Temperature-Pressure Detection. *ACS Appl. Mater. Interfaces* **2017**, *9*, 39484–39492.
- (32) Ito, H.; Muraoka, Y.; Yamazaki, T.; Imamura, T.; Mori, H.; Ichida, M.; Sumida, M.; Matsubara, F. Structure and Chemical Composition of Silk Proteins in Relation to Silkworm Diet. *Text. Res. J.* **1995**, *65*, 755–759.
- (33) Xu, L. P.; Chen, Y.; Yang, G.; Shi, W.; Dai, B.; Li, G.; Cao, Y.; Wen, Y.; Zhang, X.; Wang, S. Ultratrace DNA Detection Based on the Condensing-Enrichment Effect of Superwetttable Microchips. *Adv. Mater.* **2015**, *27*, 6878–6884.
- (34) Pan, K.; Zhang, L.; Qian, W.; Wu, X.; Dong, K.; Zhang, H.; Zhang, S. A Flexible Ceramic/Polymer Hybrid Solid Electrolyte for Solid-State Lithium Metal Batteries. *Adv. Mater.* **2020**, *32*, 2000399.
- (35) Pleul, D.; Frenzel, R.; Eschner, M.; Simon, F. X-ray photoelectron spectroscopy for detection of the different Si-O bonding states of silicon. *Anal. Bioanal. Chem.* **2003**, *375*, 1276–81.
- (36) Supuren, G.; Oglakcioglu, N.; Ozdil, N.; Marmarali, A. Moisture management and thermal absorptivity properties of double-face knitted fabrics. *Text. Res. J.* **2011**, *81*, 1320–1330.
- (37) Ling, S.; Qin, Z.; Li, C.; Huang, W.; Kaplan, D. L.; Buehler, M. J. Polymorphic regenerated silk fibers assembled through bioinspired spinning. *Nat. Commun.* **2017**, *8*, 1387.
- (38) Ling, S.; Li, C.; Jin, K.; Kaplan, D. L.; Buehler, M. J. Liquid Exfoliated Natural Silk Nanofibrils: Applications in Optical and Electrical Devices. *Adv. Mater.* **2016**, *28*, 7783–7790.
- (39) Yang, Y.; Song, Y.; Bo, X.; Min, J.; Pak, O. S.; Zhu, L.; Wang, M.; Tu, J.; Kogan, A.; Zhang, H.; Hsiai, T. K.; Li, Z.; Gao, W. A laser-engraved wearable sensor for sensitive detection of uric acid and tyrosine in sweat. *Nat. Biotechnol.* **2020**, *38*, 217–224.
- (40) Yu, Y.; Nassar, J.; Xu, C.; Min, J.; Yang, Y.; Dai, A.; Doshi, R.; Huang, A.; Song, Y.; Gehlhar, R.; Ames, A. D.; Gao, W. Biofuel-powered soft electronic skin with multiplexed and wireless sensing for human-machine interfaces. *Sci. Robot.* **2020**, *5*, eaaz7946.